Healing of Defects at the Interface of Nematic Liquid Crystals and Structured Langmuir-Blodgett Monolayers

Núria Petit-Garrido,[1,2] Rahul P. Trivedi,[2] Jordi Ignés-Mullol,[1,*] Josep Claret,[1] Clayton Lapointe,[2] Francesc Sagués,[1] and Ivan I. Smalyukh[2,3,†]

[1]*SOC&SAM group, IN²UB, and Departament de Química Física, Universitat de Barcelona, Martí i Franquès 1, 08028 Barcelona, Catalonia, Spain*

[2]*Department of Physics and Liquid Crystal Materials Research Center, University of Colorado, Boulder, Colorado 80309, USA*

[3]*Renewable and Sustainable Energy Institute, National Renewable Energy Laboratory and University of Colorado, Boulder, Colorado 80309, USA*

(Received 31 March 2011; published 17 October 2011)

We use Langmuir-Blodgett molecular monolayers and nematic liquid crystals as model two- and three-dimensional orientationally ordered systems to study the stability and healing of topological defects at their contact interfaces. Integer-strength defects at the monolayer induce disclinations of similar strength in the nematic that, however, do not propagate deep into the bulk, but rather form single- or double-split arch-shaped loops pinned to the interface. This behavior is qualitatively independent of the far-field director orientation and involves either half-integer singular or twist-escaped unity-strength nonsingular nematic disclinations. These two defect configurations can be selected by varying sample preparation given their comparable free energy, consistently with direct probing by use of laser tweezers.

DOI: 10.1103/PhysRevLett.107.177801 PACS numbers: 61.30.Jf, 61.30.Hn, 61.30.Pq

Topological defects are ubiquitous features of orientational and partial translational ordering systems [1–9]. Defects in soft matter systems such as liquid crystals (LCs) and surfactant monolayers can mediate phase transitions [1,2], enable the existence of frustrated thermodynamic phases such as the blue phases and the twist grain boundary phase [1], and are useful as model systems for the dynamics of the early-universe cosmic strings [3,4]. Defects in LCs arise spontaneously upon transitions into higher order phases or as a result of boundary conditions in widely used confined geometries. Recent studies have been directed towards understanding the defects and healing of the disorder induced by confining surfaces [10] or colloidal inclusions in the LC bulk [5]. Controlled generation of multistable textures that include disclination lines has been achieved by patterning surface boundary conditions using microengineered surfaces [11–13]. On the other hand, patterning of LC alignment and generation of defects via interfacial contact with other soft matter systems exhibiting broken symmetries and topological defects is rarely explored [14]. Understanding textures and defects in LCs in contact with structured and random soft surfaces is also important for the development of novel biodetection techniques [15,16].

Here we utilize Langmuir-Blodgett (LB) molecular monolayers [17] and nematic LCs as model 2D and 3D orientationally ordered systems, respectively. By use of three-dimensional optical imaging, we show that the pattern of molecular alignment in the monolayer is effectively transferred to the LC. Line defects induced in the LC bulk form ''arches'' that either escape in the third dimension or split into lower-strength disclinations. We explore the effects of far-field director alignment and explain the experimental findings by analyzing the free energy costs of these structures.

Glass substrates of an area of a few square centimeters are patterned by LB transfer of a ''two-dimensional emulsion'' of the surfactant 4-[4-[4-octylphenyl/azo]-phenoxy] butanoic acid (8Az3COOH). These films are previously self-assembled at the air-water interface [18], where they organize into isolated submillimeter circular islands featuring polar nematic order with the elongated molecules anchored at a fixed angle of the interface normal ($\sim 45°$), and a tilt orientation tangential to the circular boundary ($s = +1$, $c = \pi/2$), which results in a selectable orientational chirality, either clockwise (CW) or counterclockwise (CCW) [19]. In contact with the LB-coated glass substrate, LC molecules follow the local in-plane orientation of the amphiphilic molecules in the monolayer [20]. This procedure, in which LC molecules are aligned by self-assembled patterns featuring a well-defined and robust tilt-orientational order in a monolayer of uniform thickness, is in contrast to other patterning techniques based on mechanical [21] or optical [22] modification of a polymer layer, which lacks a similar degree of order.

We assemble LC cells that impose uniform boundary conditions on the complementary plate, away from the LB-coated plate. Uniform planar anchoring is achieved by means of a rubbed, spin-coated layer of polyimide (PI-2555, HD MicroSystems) and vertical anchoring conditions by treatment of the glass plate with a dilute (< 2 wt %) aqueous solution of DMOAP (*N, N*-dimethyl-*n*-octadecyl-3aminopropyl-trimethoxysilyl chloride, Sigma Aldrich). Monodisperse silica beads between the glass

plates act as spacers. Thickness effects are explored in the range 5–60 μm. Cells are filled by capillarity either with pentylcyanobiphenyl (5CB, Frinton Labs) or with the nematic mixture E7 (Merck). The filling direction is kept parallel to the rubbing direction in cells having substrates with planar anchoring. For fluorescence confocal polarizing microscopy (FCPM) [23,24] and two-photon excitation fluorescence polarizing microscopy (2PEFPM) [25,26] studies, we used a low-birefringence nematic LC mixture (ZLI-2806, EM Chemicals) doped with about 0.01 wt % of the fluorescent dye *n, n′*-bis(2,5-di-tert-butylphenyl)-3,4,9,10-perylenedicarboximide (BTBP, Aldrich).

Polarizing optical microscopy images are obtained using a Nikon Eclipse 50i microscope. FCPM and 2PEFPM images are obtained by use of an integrated multimodal imaging setup built around an Olympus IX-71 inverted microscope [25]. For fluorescence excitation in FCPM, we use a 488 nm Ar ion laser. Two-photon excitation in 2PEFPM is performed by use of a 980 nm pulsed laser beam from a tunable (680–1080 nm) femtosecond laser with a Ti:sapphire oscillator (140 fs, 80 MHz, Chameleon Ultra-II, Coherent). Excitation intensity is kept minimal in all cases to avoid altering the photosensitive LB films and the director structures in the LC. Imaging is performed with collinear polarization directions for excitation and detected fluorescence light. The transition dipole moments of absorption and emission of the anisotropic BTBP dye molecules follow the nematic director $\mathbf{n}(\mathbf{r})$ [23]. Therefore, fluorescence intensity in the images scales as $\cos^4\theta$ in FCPM and as $\cos^6\theta$ in 2PEFPM, where θ is the angle between the polarization of probing light and $\mathbf{n}(\mathbf{r})$ [23–26]. Information about the spatial variation in the orientation of $\mathbf{n}(\mathbf{r})$ is extracted by comparing images acquired for different polarization directions of probing light. Using 2PEFPM is advantageous with respect to FCPM, particularly in thick samples, given its improved sensitivity and deeper penetration into the sample [25,26].

Polarizing microscopy of hybrid planar–LB-coated LC cells reveals that $\mathbf{n}(\mathbf{r})$ features isolated domains surrounded by uniformly aligned LC, which correlates with the known structure of the precursor monolayer [18]. The LC pretilt angle is estimated to be 35°–40° on the LB-coated plate and less than 5° on the polyimide-coated plate. The combination of temperature cycling, chirality of underlying LB disks, and nematic LC flow direction during the cell filling fully determine the structure of $\mathbf{n}(\mathbf{r})$ [Figs. 1(a)–1(d)]. If the cell is filled with LC in the nematic phase, the domains feature a single disclination loop, which is stable over time, normal to the far-field director, and connects the center and the periphery of the LB domain [Figs. 1(a) and 1(b)]. The disclination appears in the region where nematic flow during filling is antiparallel to the head-to-tail orientation of surfactant molecules in the underlying LB film. For example, if the cell is filled from right to left (“east to west”) the disclination is to the “north” (“south”) of the island center for CW (CCW) domains. The polarization state of light transmitted through the sample suggests that the director twists across the cell in all regions above the LB domain except for the region radially opposite to the disclination line [dark brushes in Figs. 1(a) and 1(b)].

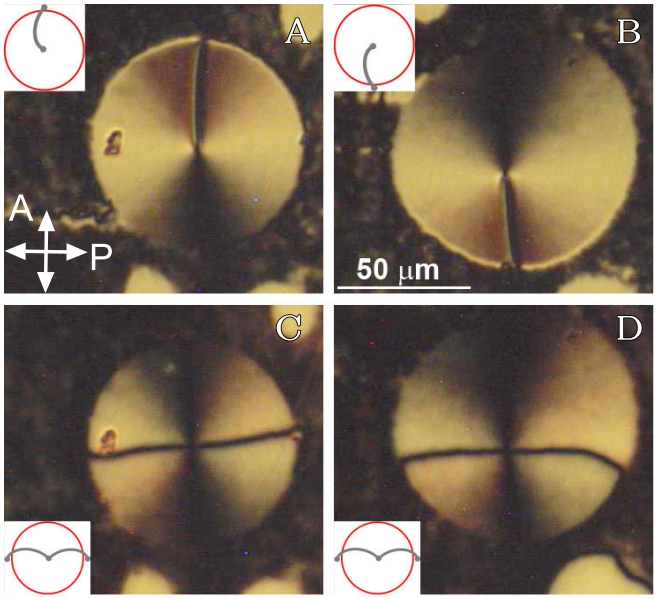

FIG. 1 (color online). Polarizing optical micrographs of the LC in contact with isolated either CW (a),(c) or CCW (b),(d) domains in the LB film. At the complementary plate, surface anchoring is uniform planar (horizontal) and the cells are filled with the nematic LC right to left. Images (c) and (d) are obtained after heating the LC into the isotropic phase and cooling it back into the nematic. The insets schematically illustrate the defect configuration. Cell thickness is 5 μm.

Heating the sample to isotropic phase or filling the cell at a temperature corresponding to the isotropic phase of the LC and then cooling down to the nematic phase alters the structure of $\mathbf{n}(\mathbf{r})$ and results in the formation of two disclination loops, both parallel to the far-field director and connecting the defect of the LB island with its periphery [Figs. 1(c) and 1(d)]. This structure is also stable over time. Unlike the single-loop case, orientational chirality of the underlying LB domain is not reflected in the polarizing microscopy textures. Linearly polarized incident light traversing the island region remains linearly polarized but with the polarization rotated to be along the domain boundary.

In order to gain insight into the director configurations and defect structures described above, we perform direct 3D imaging of $\mathbf{n}(\mathbf{r})$ by means of FCPM and 2PEFPM. Figure 2 shows FCPM images of an isolated single-loop island, analogous to Fig. 1(b). The images reveal that the single loop is an integer-strength twist-escaped disclination that connects $+1$ and -1 boojums located at the center of the LB domain and its periphery, respectively. This nonsingular defect line extends into the LC bulk and

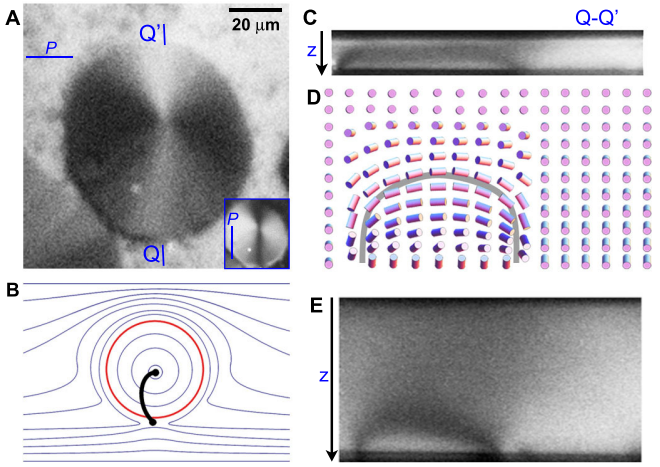

FIG. 2 (color online). Single-loop defect structures. In-plane (a) and vertical (c),(e) FCPM sections of an isolated LC domain with planar anchoring on the complementary plate. (b),(d) Director field within the (b) in-plane and (d) vertical cross sections. The sample thickness (distance between black stripes corresponding to glass plates) is 10 μm in (c) and 60 μm in (e). The thick arch-shaped lines in (b),(d) depict the defect lines.

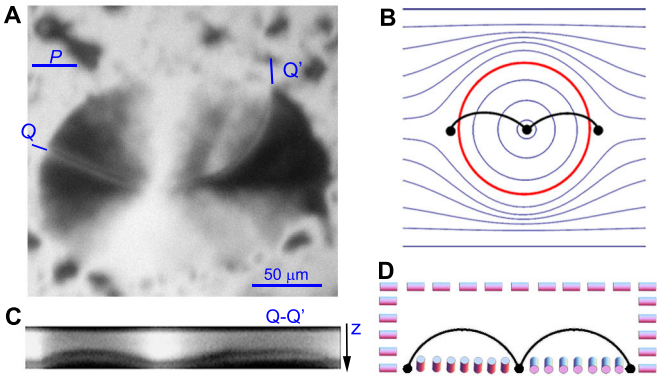

FIG. 3 (color online). In-plane (a) and vertical (c) FCPM cross sections of a cell with an isolated LC domain with the double-loop configuration in a 6 μm thick cell with uniform planar anchoring on the complementary plate. (b),(d) Schematics of $\mathbf{n}(\mathbf{r})$ in (b) in-plane and (d) vertical cross sections. The arch-shaped lines in (b),(d) depict the half-integer defect lines.

then returns back to the surface by forming an "arch" [Fig. 2(c)]. The Q-Q' cross section in Fig. 2(c) shows that $\mathbf{n}(\mathbf{r})$ in the arch region is along the far-field director (horizontal in the images) near the PI-coated plate, twists until it becomes orthogonal to this direction a few microns away from the LB film, and then twists further until it is parallel to the in-plane projection of the surfactant molecules on the LB-coated plate. A schematic of the reconstructed LC configuration is shown in Fig. 2(b) for the in-plane section and in Fig. 2(d) for the vertical cross section containing this twist-escaped disclination. The local twist of $\mathbf{n}(\mathbf{r})$ across the cell is determined by the path along which there are minimal distortions between the far-field uniform director and the local head-to-tail orientation of the surfactant molecules on the LB film. The twist across the cell is maximum (180°) in the disclination region and zero in the region opposite to it [27]. The penetration depth of the director distortions into the LC bulk is typically half the sample thickness if the latter is less than about 10 μm [Fig. 2(c)]. For thicker samples, the director distortions and the ensuing defect structures are independent of sample thickness [Fig. 2(e)].

Figure 3 shows FCPM images of an isolated LB domain with the double-loop configuration, analogous to Figs. 1(c) and 1(d), and reveals two pinches (disclination dipoles passing through an interface [28]) connected by arch-shaped $s = 1/2$ disclination semiloops pinned to the center of the LB domain [28] and connecting it to the opposite poles of the domain periphery along the far-field director. The penetration depth for these semiarches is smaller than for the arch in single-loop domains and the maximum twist across the cell is now $\pi/2$ in the disclination region, where the tangent to the circular boundary is perpendicular to the far-field director (Fig. 3).

To unravel the influence of the orientation of the far-field director and confinement on the observed defects and structures, we have explored cell thickness ranging from 5 to 40 μm with vertical boundary conditions for $\mathbf{n}(\mathbf{r})$ on the complementary confining glass plate. Figure 4 shows 2PEFPM images of a 30 μm thick sample, both after filling the cell with the nematic LC and after heating it to the isotropic phase and cooling it down. Interestingly, the defect structures formed near the LB plate are qualitatively

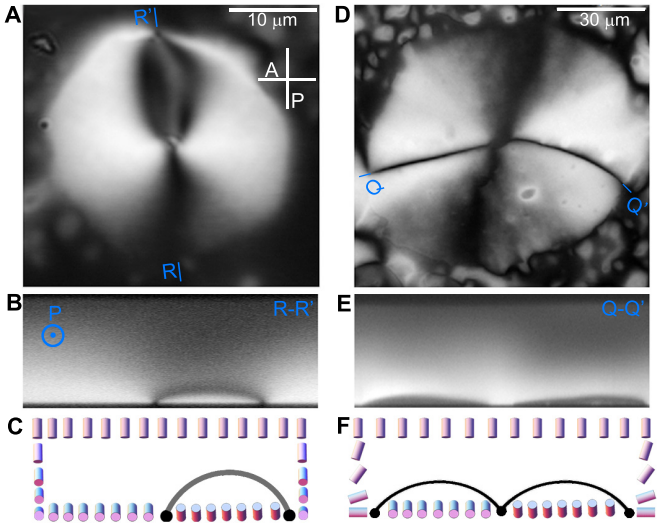

FIG. 4 (color online). Single (a)–(c) and double (d)–(f) disclination loops above a CW LB domain in a 30 μm thick sample with homeotropic anchoring on the complementary plate probed by 2PEFPM. (a),(d) Monochromatic polarizing microscopy images, (b),(e) 2PEFPM vertical cross sections marked in (a),(d), and (c),(f) corresponding schematics of the director structures. The thick line in (c) and the thin line in (f) depict the nonsingular twist-escaped and half-integer singular defect lines, respectively.

similar to what we have described when using planar far-field boundary conditions: arches of either one twist-escaped nonsingular $s = 1$ [Figs. 4(a)–4(c)] or two singular $s = 1/2$ disclinations connecting the center of the LB domain and its periphery [Fig. 4(d) and 4(f)], showing similar dependence on the sample preparation as the planar cells. The depth of defect penetration into the LC bulk is comparable to the planar anchoring case, except for cells thinner than about 5 μm, when one observes a single $s = 1$ disclination spanning across the cell gap from the center of the LB island to the complementary glass plate, irrespectively of sample preparation [27].

One can generate similar boundary conditions at the centimeter scale using a so-called theta cell [29] constructed by combining a circularly rubbed polyimide-treated glass plate with one that is unidirectionally rubbed. We find that the $\mathbf{n}(\mathbf{r})$ pattern qualitatively resembles the double-loop configuration [Fig. 1(c) and 1(d)], regardless of sample preparation or handedness of the circular rubbing. This may suggest that the stability of the defect structures depends on the size of the circular domains, although we see no size dependence for domains 30–200 μm in diameter. We note that an important role might be played by the different values of director pretilt at the LB-LC (35°–40°) and polyimide-LC interfaces ($< 5°$).

A semiquantitative analysis suggests that the two configurations described above have comparable elastic energies. The free energy of a singular $s = +1/2$ disclination can be approximated as $F_{1/2} \approx \pi \frac{1}{4} Kl \ln[h/(2r_c)] + F_{\text{core}}$, and that of a nonsingular twist-escaped $s = +1$ disclination as $F_1 \approx 3\pi Kl$ [30]. Here, l is the disclination length, h is the sample thickness, K is the average Frank elastic constant, r_c is the radius of the defect core (in the nm range), and F_{core} is the defect core energy. Using $K \approx 12$ pN (ZLI-2806), one can roughly estimate the energy per unit length (line tension), $T_{1/2} \approx 60$ pN, and $T_1 \approx 113$ pN. For typical values of l, we obtain an estimate $F \sim (1\text{–}5) \times 10^{-15}$ J $\gg k_B T$, similar for the two types of configurations since the twist-escaped $s = 1$ disclination is typically 10%–20% longer than each of the two $s = 1/2$ defect lines. The energy barrier for a transition between the two configurations is likely to also be much larger than $k_B T$, so the two structures remain stable once they appear, depending on sample preparation. We note that this is in contrast to recent studies of healing of disorder induced by rough confining surfaces [31–33], which involve energetic barriers too weak to generate topological defects.

An experimental rough estimate for the above energy value can be obtained through manipulation of the defect lines with tightly focused linearly polarized laser beams [34,35]. We find that the disclination ends are strongly pinned to the LB-coated surface and remain intact as they are stretched orthogonally by optical tweezers operating at 1064 nm. At laser powers of up to 30 mW, one can stretch the disclinations up to 10% for singular half-integer lines and up to about 5% for the nonsingular twist-escaped defects. For the used parameters of the laser trap and material parameters of the system, we estimate that the maximum polarization-dependent force that can be exerted by the trap on a localized liquid crystal structure [36] is in the range 30–65 pN, depending upon the defect structure and laser polarization. From the balance of optical gradient force and defect line tension [36], we get $T_{1/2} \approx 55\text{–}75$ pN, and $T_1 \approx 95\text{–}115$ pN, comparable to the line tensions of similar defects in the LC bulk [28,30] and consistent with the above estimates.

To conclude, by use of direct 3D imaging and laser tweezers, we have described the healing of defects imposed in a nematic LC by contact with a self-assembled ordered surfactant monolayer. We have demonstrated that healing occurs via formation of single escaped or double singular arch-shaped defect loops independently of far-field boundary conditions. This defect healing scenario is expected to persist in all situations when a nematic liquid crystal is strongly anchored to a 2D soft matter system with polar nematic order. Further experimental work is required to assess the universality of our results when either the lateral order of the monolayer or the symmetry of the bulk liquid crystal is modified.

This work has been partially supported by MICINN (Project FIS2006-03525), DURSI (Project 2009 SGR 1055), and by the NSF Grants No. DMR-0820579, No. DMR-0844115, No. DMR-0645461, and No. DMR-0847782. N. P.-G. acknowledges support from MICINN (Grant No. AP2007-01103 and a travel grant). We thank Noel Clark and Leo Radzihovsky for discussions and Taewoo Lee for help with imaging experiments.

*jignes@ub.edu
†ivan.smalyukh@colorado.edu

[1] P. M. Chaikin and T. C. Lubensky, *Principles of Condensed Matter Physics* (Cambridge University Press, Cambridge, England, 1995).
[2] A. M. Alsayed *et al.*, Science **309**, 1207 (2005).
[3] M. J. Bowick *et al.*, Science **263**, 943 (1994).
[4] I. Chuang *et al.*, Science **251**, 1336 (1991).
[5] P. Poulin *et al.*, Science **275**, 1770 (1997).
[6] L. Ramos *et al.*, Phys. Rev. E **66**, 031711 (2002).
[7] M. Zapotocky *et al.*, Science **283**, 209 (1999).
[8] P. Schall *et al.*, Science **305**, 1944 (2004).
[9] P. Schall *et al.*, Nature (London) **440**, 319 (2006).
[10] J. Fukuda and S. Zumer, Nature Commun. **2**, 246 (2011).
[11] Y. S. Choi *et al.*, Phys. Rev. E **80**, 060701 (2009).
[12] J. H. Kim, M. Yoneya, and H. Yokoyama, Nature (London) **420**, 159 (2002).
[13] I. Dozov, M. Nobili, and G. Durand, Appl. Phys. Lett. **70**, 1179 (1997).
[14] H. Yokoyama, Proceedings of the 23rd International Liquid Crystal Conference, Crakow, 2010, Abstract No. P1.147 (to be published).

[15] S. J. Woltman, G. D. Jay, and G. P. Crawford, Nature Mater. **6**, 929 (2007).
[16] J. M. Brake *et al.*, Science **302**, 2094 (2003).
[17] M. C. Petty, *Langmuir-Blodgett Films: An Introduction* (Cambridge University Press, Cambridge, England, 1996).
[18] J. Ignes-Mullol *et al.*, Langmuir **21**, 2948 (2005).
[19] N. Petit-Garrido *et al.*, Phys. Rev. Lett. **103**, 237802 (2009).
[20] J. Fang *et al.*, Langmuir **15**, 297 (1999).
[21] J. H. Kim *et al.*, Appl. Phys. Lett. **78**, 3055 (2001).
[22] J. I. Niitsuma, M. Yoneya, and H. Yokoyama, Appl. Phys. Lett. **92**, 241120 (2008).
[23] I. I. Smalyukh, S. V. Shiyanovskii, and O. D. Lavrentovich, Chem. Phys. Lett. **336**, 88 (2001).
[24] I. I. Smalyukh, Mol. Cryst. Liq. Cryst. **477**, 23 (2007).
[25] T. Lee, R. P. Trivedi, and I. I. Smalyukh, Opt. Lett. **35**, 3447 (2010).
[26] R. P. Trivedi *et al.*, Opt. Express **18**, 27658 (2010).
[27] N. Petit-Garrido (to be published).
[28] M. Kléman, *Points, Lines, and Walls: In Liquid Crystals, Magnetic Systems, and Various Ordered Media* (J. Wiley, Chichester, England, 1983).
[29] M. Stalder and M. Schadt, Opt. Lett. **21**, 1948 (1996).
[30] P. E. Cladis and M. Kleman, J. Phys. (Paris) **33**, 591 (1972).
[31] Q. Zhang and L. Radzihovsky, Phys. Rev. E **81**, 051701 (2010).
[32] L. Radzihovsky and Q. Zhang, Phys. Rev. Lett. **103**, 167802 (2009).
[33] M. Nespoulous, C. Blanc, and M. Nobili, Phys. Rev. Lett. **104**, 097801 (2010).
[34] I. I. Smalyukh *et al.*, Nature Mater. **9**, 139 (2009).
[35] C. P. Lapointe, T. G. Mason, and I. I. Smalyukh, Science **326**, 1083 (2009).
[36] I. I. Smalyukh *et al.*, Opt. Express **15**, 4359 (2007).